Early formation of GABAergic synapses governs the development of adult-born neurons in the olfactory bulb

Pallotto, Marta ; Nissant, Antoine ; Fritschy, Jean-Marc ; Rudolph, Uwe ; Sassoè-Pognetto, Marco ; Panzanelli, Patrizia ; Lledo, Pierre-Marie

Abstract: In mammals, olfactory bulb granule cells (GCs) are generated throughout life in the subventricular zone. GABAergic inputs onto newborn neurons likely regulate their maturation, but the details of this process remain still elusive. Here, we investigated the differentiation, synaptic integration, and survival of adult-born GCs when their afferent GABAergic inputs are challenged by conditional gene targeting. Migrating GC precursors were targeted with Cre-eGFP-expressing lentiviral vectors in mice with a floxed gene encoding the GABA(A) receptor 2-subunit (i.e., Gabra2). Ablation of the 2-subunit did not affect GC survival but dramatically delayed their maturation. We found a reduction in postsynaptic 2-subunit and gephyrin clusters accompanied by a decrease in the frequency and amplitude of GABAergic postsynaptic currents beginning 14 d post-injection (dpi). In addition, mutant cells exhibited altered dendritic branching and spine density. Spine loss appeared with mislocation of glutamatergic synapses on dendritic shafts and a reduction of spontaneous glutamatergic postsynaptic currents, underscoring the relevance of afferent GABAergic transmission for a proper synaptic integration of newborn GCs. To test the role of GABAergic signaling during much early stages of GC maturation, we used a genetic strategy to selectively inactivate Gabra2 in precursor cells of the subventricular zone. In these mice, labeling of newborn GCs with eGFP lentiviruses revealed similar morphological alterations as seen on delayed Gabra2 inactivation in migrating neuroblasts, with reduced dendritic branching and spine density at 7 dpi. Collectively, these results emphasize the critical role of GABAergic synaptic signaling for structural maturation of adult-born GCs and formation of glutamatergic synapses.

DOI: https://doi.org/10.1523/JNEUROSCI.0214-12.2012

Early formation of GABAergic synapses controls the development of adult-born neurons in the olfactory bulb

Running Head: Maturation of adult-born neurons

Marta Pallotto[1,2,3], Antoine Nissant[2,3], Jean-Marc Fritschy[4], Uwe Rudolph[5], Marco Sassoè-Pognetto[1], Patrizia Panzanelli[1], and Pierre-Marie Lledo[2,3]

[1]Department of Anatomy, Pharmacology and Forensic Medicine and National Institute of Neuroscience-Italy, University of Turin, Italy.

[2]Institut Pasteur, Laboratory for Perception and Memory, Department of Neurosciences, *F*-75015 Paris, France.

[3]Centre National de la Recherche Scientifique (CNRS), Unité de Recherche Associée (URA2182), *F*-75015 Paris, France.

[4]Institute of Pharmacology and Toxicology, University of Zurich and Neuroscience Center Zurich, CH - 8057 Zurich, Switzerland.

[5]Laboratory of Genetic Neuropharmacology, McLean Hospital, and Department of Psychiatry, Harvard Medical School, Belmont, MA 02478-1064, USA.

Correspondence:
Dr. Pierre-Marie Lledo, Institut Pasteur, Perception and Memory laboratory, 25 rue du Dr. Roux, *F*-75724 Paris Cedex 15, France. E-mail: pmlledo@pasteur.fr
Dr. Marco Sassoè-Pognetto, Department of Anatomy, Pharmacology and Forensic Medicine, University of Turin, and Istituto Nazionale di Neuroscienze, Corso Massimo d'Azeglio 52, I-10126 Torino, Italy. E-mail: marco.sassoe@unito.it

Senior Editor: Dr. Mark Bothwell, Univ Washington MS: Box 358056, Dept. of Physiology & Biophysics, Seattle, WA, WA 98195-8056

Figures: **6**	Tables: **7**	Pages: **34**
Words in the Abstract: **238**	Introduction: **514**	Discussion: **1,572**

Key Words: Dendrites; $GABA_A$ receptor; Glutamate; Granule cells; Adult neurogenesis; Spines.

Acknowledgements: The life insurance company "Arpège", the "Fondation pour la Recherche Médicale" (FRM Team) and the Agence Nationale de la Recherche "ANR-BLAN-SVSE4-LS-110624" and "ANR-09-NEUR-004" in the frame of "ERA-NET NEURON" of FP7 program by the European Commission supported Lledo's lab. MP is the recipient of fellowships sponsored by Università Italo-Francese and by Institut Servier; JMF was supported by Swiss National Science Foundation Grant 31003A_130495; PP by Compagnia di San Paolo (grant 2008-2254) and MSP by the Compagnia di San Paolo (2007) and Regione Piemonte (Ricerca Sanitaria Finalizzata 2008/bis).

Abstract

Olfactory bulb granule cells (GCs) are generated throughout life in the rodent subventricular zone. The role of GABAergic signaling in this process remains elusive. Using conditional gene targeting in adult mice to functionally disrupt afferent GABAergic synaptic transmission in newborn GCs, we investigated their survival, differentiation, and synaptic integration. In mice with floxed *Gabra2* alleles, migrating newborn GC precursors were targeted with Cre-eGFP-expressing lentiviral vectors. Ablation of the α2-subunit did not affect GC survival but delayed dramatically their maturation. A reduction in postsynaptic α2-subunit and gephyrin clusters and in the frequency and amplitude of GABAergic postsynaptic currents became detectable around 14 days post-injection (dpi) and persisted thereafter. In mutant cells, dendritic branching and spine density were reduced thereafter. Spine loss was accompanied by mislocation of glutamatergic synapses on dendritic shafts and reduction of spontaneous excitatory postsynaptic currents, underscoring the relevance of afferent GABAergic transmission for synaptic integration of newborn GCs. To test the role of GABAergic signaling during early stages of GC maturation, we used a genetic strategy to selectively target *Gabra2* precursor cells of the subventricular zone. In these mice, labeling of newborn GCs with eGFP-lentiviruses revealed very similar morphological alterations as seen upon delayed *Gabra2* inactivation, with reduced dendritic branching and spine density already at 7 dpi. These results underscore the key role of GABAergic synaptic signaling for newborn GC maturation and reveal the unexpected function of GABAergic inputs in controlling the formation of glutamatergic synapses.

Introduction

As a unique form of structural plasticity, adult neurogenesis sculpts neuronal circuit functions by continuously adding newly formed neurons to preexisting networks. In turn, this process depends on the overall synaptic activity of the host network (Kelsch et al., 2010; Ming and Song, 2011). Key parameters regulating adult neurogenesis likely include the properties of early synapses impinging onto developing adult-born neurons. Also, the mechanisms linking synaptogenesis with morphological differentiation and functional maturation are of particular interest because they represent major facets of synaptic plasticity and condition the long-term survival of newborn neurons (Yamaguchi and Mori, 2005; Whitman and Greer, 2007; Kelsch et al., 2008; Nissant et al., 2009).

Neurogenic niches persist in the dentate gyrus of the hippocampus and the subventricular zone (SVZ) of the adult rodent brain (Altman, 1969; Alvarez-Buylla and Garcia-Verdugo, 2002; Kempermann et al., 2004). Neuroblasts generated in the SVZ migrate along the rostral migratory stream (RMS) to reach the olfactory bulb (OB), where they differentiate as granule cells (GCs) and periglomerular cells and integrate functionally over several weeks (Lledo et al., 2006). GCs are axonless GABAergic interneurons; their apical dendrites extends radially into the external plexiform layer (EPL) and bears numerous spines that establish reciprocal synapses with the dendrites of mitral cells and tufted cells (Shepherd et al., 2007). In addition, GCs receive various axo-dendritic excitatory synapses, as well as inhibitory synapses from local microcircuits. GABAergic signaling regulates early steps of adult neurogenesis (Platel et al., 2008; Ming and Song, 2011); however, its relevance for the maturation and synaptic integration of newborn GCs is unknown. Recently, we have demonstrated that newborn GCs form functional GABAergic and glutamatergic synapses shortly after entering the OB, with an initial predominance of GABAergic synapses (Panzanelli et al., 2009; Katagiri et al., 2011). This observation raised the possibility that GABAergic synaptic transmission regulates the morphological and functional maturation of GCs, known to be under control of activity-dependent mechanisms (Kelsch et al., 2010; Ming and Song, 2011).

We took advantage of the selective expression of $GABA_A$ receptors ($GABA_AR$) containing the α2-subunit in GCs (Panzanelli et al., 2009) to irreversibly alter synaptic GABAergic inputs in adult-born GCs by conditional deletion of *Gabra2* in two distinct experiments. First, cell-specific *Gabra2* ablation was achieved in neuroblasts on their way to the OB by injecting a lentiviral vector encoding Cre-eGFP into the RMS of mice carrying

floxed *Gabra2* alleles. Morphological development of mutant GCs and formation of functional synapses were analyzed by immunohistochemistry and electrophysiology. These experiments revealed impaired GABAergic synaptic responses in mutant cells and striking defects in dendritic development and spine formation, without curtailing GC survival. The impact of *Gabra2* inactivation on plasticity produced by chronic olfactory deprivation and enrichment was tested to unravel possible contributions of GABAergic synaptic transmission to the experience-sensitive regulation of GC development. Second, using the Tet-on system in double transgenic mice, *Gabra2* deletion was induced in progenitor cells expressing GLAST, yielding results comparable to the first experiment. Collectively, these data reveal that early GABAergic synapses set the degree of activity-dependent regulation of adult-born GCs development and influences their synaptic integration into pre-existing networks.

Materials and Methods

Animals. All experiments were conducted in accordance with the European Communities Council Directive of 24 November 1986 (86/609/EEC) and with institutional approval. The generation of mice carrying the gene for *Gabra2* flanked by LoxP sites (hereafter called α2-FL) has been described previously (Witschi et al., 2011). These transgenic mice were back-crossed on the C57BL/6J background for more than nine generations. Homozygous α2-FL mice were used for conditional deletion of *Gabra2* by Cre-eGFP lentiviral transduction of neuroblasts migrating through the RMS, with wild-type (WT) mice as control. In a second series of experiments, $\alpha2^{fl/fl}$–GLAST::CreERT2$^{+/-}$ transgenic mice were obtained by cross-mating GLAST::CreERT2 mice (Mori et al., 2006) with α2-FL mice. In these double-mutant mice, hereafter called α2-Glast, *Gabra2* deletion was induced in GLAST-expressing progenitor cells upon systemic tamoxifen administration. Control mice were injected with vehicle (corn oil). Mice were housed under a 12h light/dark cycle, with food and water available *ad libitum*.

Lentiviral vectors. A replication-deficient lentiviral vector was used to express the CRE recombinase and eGFP in newborn GCs of α2-FL and WT control mice. We used a plasmid generously provided by Tyler Jacks (Addgene, Plasmid 20781: UbC-GFP.PGK-Cre vector). The concentration of lentiviral vector particles used was 115 ng of P24/µL (the p24 protein is a nucleocapsid protein used as an important early marker of HIV infection). Average vector titers were in the order of 10^9 transduction units/ml. For visualization of eGFP in newborn GC of α2-Glast mice, we used a custom-built lentivirus driven by the phosphoglycerate kinase (PGK) promoter as previously described (Grubb et al., 2008).

Stereotaxic injections. Adult male mice aged between 8 and 12 weeks at the time of virus injection were used for morphological analyses (n=94) and electrophysiological recordings (n=48). Mice were anesthetized with an i.p. injection of xylazine (Rompun, Bayer Health Care) and ketamine (Imalgene, Merial) dissolved in PBS at a dose of 10 mg/kg and 120 mg/kg respectively, and mounted on a stereotaxic apparatus (Kopf). We performed bilateral injections into the RMS at the following coordinates, using Bregma as reference: mediolateral ±0.82 mm, anteroposterior +3.3 mm, and -2.90 mm from the pial surface (Panzanelli et al., 2009). Viral vector particles (200 nL per site) were injected using a nanoliter injector Nanoject II (Drummond Scientific Company) with a glass micropipette at a rate of 23 nL/s. Animals were killed at the indicated survival times after virus injection (dpi = days post injection).

Olfactory enrichment and deprivation.

Chemical ablation of olfactory epithelium. Seven days after lentivirus injection, α2-FL and WT mice were given one i.p. injection of dichlobenil (2,6-dichlobenzonitrile, 25 µg/g body weight; Fluka) in dimethyl sulfoxide (DMSO; 2 µL/g body weight) or vehicle as control as previously described (Vedin et al., 2004). Mice were sacrificed at 30 dpi. The efficacy of this sensory deafferentation protocol was confirmed by assessing the decrease of tyrosine-hydroxylase (TH) immunoreactivity in the glomerular layer of the OB (Stone et al., 1991)(data not shown).

Olfactory enrichment. Starting seven days after viral injection, mice were exposed daily to three different aromatic fragrances (Table 1) during three weeks (Rochefort et al., 2002). The odorants were placed inside a tea ball on the cage floor. In the control group, empty tea balls were placed in the cage. Mice were killed for analysis after 30 dpi.

Tissue processing for immunohistochemistry Two different protocols were used for optimal detection of the markers to be analyzed:

Shortly-fixed tissue: Mice were deeply anesthetized (sodium pentobarbital; 50 mg/kg i.p.; Sanofi-Aventis) and decapitated. The OB was dissected out, collected in ice-cold artificial cerebrospinal fluid (ACSF) and cut in 300 µm-thick horizontal slices with a sliding microtome (Leica, VT 1000S), as described previously (Schneider Gasser et al., 2006). Slices were incubated in oxygenated ACSF for 30 min at 35°C, fixed by immersion in 4% paraformaldehyde at room temperature for 12 min, cryoprotected in 30% sucrose, flat-frozen, and sectioned with a cryostat (Microm HM 560). The 16 µm-thick cryosections were mounted onto gelatine-coated glass slides and stored at –20°C.

Perfused tissue: Mice were anesthetized as above and fixed by intracardiac perfusion of PBS, followed by ice-cold 4% formaldehyde in 0.1 M sodium phosphate buffer, pH 7.4. The brains were removed, post-fixed in the same fixative overnight and cryoprotected in 30% sucrose. The OBs were then frozen with dry-ice and cut into 50 µm-thick coronal sections with a cryostat. Sections were stored in anti-freeze solution (15% glucose and 30% ethylene glycol in 50 mM sodium phosphate buffer, pH 7.4) at –20°C.

Immunofluorescence staining. Double and triple immunofluorescence was performed by incubating tissue sections in a mixture of primary antibodies raised in different species (see Table 2), diluted in PSB with 5% normal donkey serum (Jackson Immunoresearch) and 0.05%

Triton X-100. Sections were then washed in PBS, incubated for 30 min at room temperature in secondary antibodies raised in donkey and conjugated to Alexa 488 (Invitrogen), Cy3, or Cy5 (Jackson Immunoresearch). Finally the sections were rinsed again, and mounted on glass slides using a fluorescence mounting medium (Dako).

Image acquisition and analysis. Sections were visualized by confocal laser-scanning microscopy (Zeiss LSM5 Pascal) using sequential acquisition of separate channels to avoid fluorescence cross-talk. Stacks of confocal sections were acquired with either a 40x (N.A. 1.3) or 100x objective (N.A. 1.4), with the pinhole set at 1 Airy unit. For display, images were processed with the image analysis software Imaris (version 4.3; Bitplane). All quantifications are based on least 3 animals per group and time-point after virus injection.

The dendritic morphology of newborn GCs was analyzed in 50 µm-thick sections from perfused tissue stained for eGFP. Confocal images spaced by 1 µm were acquired across the entire thickness of the section with a 40x objective and analyzed with the software Image J 1.34S (NIH, public domain). Total dendritic length and number of branches were determined on 3-D projections using the NeuronJ plug-in. Sholl analysis was performed with concentric circles spaced 10 µm and centered on the cell soma (Sholl Analysis plugin, Gosh lab). For statistical comparison, the "area under the curve" of the resulting function was calculated. Quantifications were performed on 12-15 cells from three mice of each experimental group.

Spine density was determined on apical dendritic segments of $eGFP^+$ GCs, including secondary and tertiary branches in the EPL. At least ten stacks consisting of 10–15 confocal sections acquired at high magnification were analyzed per animal using ImageJ. All dendritic protrusions with a clearly recognizable neck connected to the shaft of the dendrite were counted as spines. Measures of spine density were performed on 3-D-projected image stacks.

Preembedding immuno-electron microscopy. α2-FL mice were deeply anesthetized with sodium pentobarbital (50 mg/kg i.p.) and perfused with 2% formaldehyde and 0.1% glutaraldehyde in sodium acetate buffer, pH 6, for 2 min followed by 1 h perfusion with 2% formaldehyde and 0.1% glutaraldehyde in 0.1 M borate buffer, pH 9 (Kollo et al., 2008). The brain was taken out and postfixed in the second fixative overnight. Tissue blocks containing the OBs were cut into 80 µm coronal sections with a vibrating microtome (Leica VT 1000S). Sections were cryoprotected with 30% sucrose and frozen/thawed three times with liquid nitrogen to enhance antibody penetration. Sections were then incubated in primary antibodies against gephyrin and GFP (Table 2) diluted in Tris-buffered saline containing 10% normal

goat serum for 72 h at 4ºC. After several rinses, the sections were incubated with rabbit IgGs coupled to biotin (1:250; Vector Laboratories) and mouse IgGs coupled to 1.4 nm colloidal gold particles (1:200; Nanoprobes) for 24 h at room temperature. A standard immunoperoxidase reaction was performed to detect eGFP (Vectastain Elite; Vector Laboratories), whereas nanogold particles were visualized with the gold enhance-EM formulation (Nanoprobes), as described by the manufacturer. The sections were treated with 0.5% OsO_4 and 1% uranyl acetate, dehydrated, and embedded into Epon 812. Serial ultrathin sections were collected on copper single-hole grids and observed in a JEM-1010 transmission electron microscope (Jeol) equipped with a side-mounted CCD camera (Mega View III; Soft Imaging System) for photography.

Electrophysiology. For patch-clamp recordings, α2-FL and WT mice were deeply anesthetized with isoflurane (Mundipharma, France) and swiftly decapitated. The OB and frontal cortices were rapidly dissected and placed in ice-cold ACSF containing in mM: 124 NaCl, 3 KCl, 1.3 $MgSO_4$, 26 $NaHCO_3$, 1.25 $NaHPO_4$, 20 glucose, 2 CaCl (~310 mOsm, pH 7.3 when bubbled with a mixture of 95% O_2 and 5% CO_2; all chemicals from Sigma France). They were then glued to a block of 4% agarose and placed, submerged in ice-cold ACSF, in the cutting chamber of a vibrating microtome (Leica VT 1200S). Horizontal slices (300 µm thick) of the OBs were placed in bubbled ACSF in a warming bath at 35°C for 30 min and then at room temperature (*i.e.*, 22 ± 1°C). For whole-cell recordings, individual slices were placed in a chamber mounted on a Zeiss Axioskop upright microscope, and continuously perfused (1.5 ml/min) with room-temperature bubbled ACSF. Slices were visualized using a 40x water-immersion objective, a halogen light source, DIC filters (Zeiss, France), and a CCD camera (Hamamatsu C7500, Japan). We obtained whole-cell patch-clamp recordings from visually-targeted eGFP-labeled GCs. Patch pipettes, pulled from borosilicate glass (OD 1.5mm, ID 1.17mm, Harvard Apparatus, UK; P-87 Flaming/Brown micropipette puller, Sutter Instrument Co, UK), had resistances of 6–10 MΩ and were filled with a cesium gluconate-based solution (in mM: 126 Cs-gluconate, 6 CsCl, 2 NaCl, 10 Na-HEPES, 10 D-glucose, 0.2 Cs-EGTA, 0.3 GTP, 2 Mg-ATP, 0.2 cAMP, with 0.15% biocytin; 280–290 mOsm, pH 7.3). Rhodamine (0.1–0.4%) was included in the internal solution for $eGFP^+$ cell recordings. All membrane potentials indicated in the text are corrected for a liquid junction potential of +10mV.

Adult-born cells were identified by either double-labeling with both eGFP and rhodamine during recording or the presence of eGFP in the tip of the patch pipette after

membrane rupture. eGFP-targeted recordings that did not meet either of these criteria were discarded from our analyses. Recordings were obtained via an Axopatch 1D amplifier. Signals were Bessel filtered at 2 kHz, digitized, and sampled at intervals of 20–450 µs (2.2–50 kHz) according to the individual protocols. Compensation for fast capacitance in cell-attached mode was ~80% (12–13pF, 3–5µs); we also compensated for membrane capacitance (C_m), but not series resistance (R_s), after membrane rupture. With C_m compensation inactivated, values of C_m, R_s and membrane resistance (R_m) were estimated using peak and steady-state currents, respectively, observed in response to a 5 mV membrane step. Any experiment in which R_s changed by more than 20% was discarded from our analyses. Currents mediated by Na^+ voltage-gated channels were measured under voltage-clamp conditions. Depolarizing pulses (100 ms) from –70 mV to incremental steps (5 mV), up to +10 mV, were given at a rate of 1 Hz. Na^+ currents were measured after subtraction of scaled passive current responses to the appropriate voltage steps.

Synaptic responses were evoked using a small monopolar stimulating glass pipette (3–4 µm tip diameter, pulled from 1.5 mm OD 1.17 mm ID borosilicate glass, and filled with ACSF), finely positioned either in the GC layer (GCL) or in the EPL. Spontaneous and evoked synaptic currents were analyzed with Elphy software (Gerard Sadoc, Gif-sur-Yvette, France). The amplitude of ePSCs was measured from averaged traces (10-30 traces). Spontaneous synaptic currents were recorded during at least 5 minutes. Rise times were measured between 20 and 80% of peak amplitude. For IPSCs, decay time were derived by fitting the formula $F(t) = a*\exp(-t/t_{fast}) + b*\exp(-t/t_{slow})$, where a and b are the peak amplitude of fast and slow components, respectively, and t_{fast} and t_{slow} are the respective decay time constants. A mono-exponential fitted all EPSCs.

Statistical analyses. Data are presented as mean ± SD or ± SEM (see Tables 3-7). Statistical analyses include one-way and two-way ANOVA with post-hoc correction using Prism software (GraphPad, Prism5). For a given day post-injection (dpi), α2-FL and WT groups were compared two-by-two by Student's *t* test and Mann Whitney test.

Results

Conditional deletion of *Gabra2* causes delayed removal of α2-GABA$_A$ receptors in adult-born granule cells

GABAergic inhibition in GCs is mediated mainly by α2-containing GABA$_A$Rs (Panzanelli et al., 2009). To investigate the functional impact of GABAergic inputs in adult-born GCs, we silenced GABAergic transmission by injecting a CRE-IRES-eGFP-encoding lentivirus into the RMS of adult α2-FL mice (Fig. 1*A-B*). CRE recombinase inactivates *Gabra2* by inducing a site-specific recombination of exon 5 flanked by Lox-P sites (Panzanelli et al., 2011), while eGFP allows the visualization of transduced cells. Immunohistochemistry revealed the presence of Cre recombinase in the nucleus of eGFP$^+$ cells from 7 dpi to 90 dpi (data not shown).

We performed double-labeling for eGFP and the α2-subunit to verify the efficacy and time course of Cre-mediated deletion of *Gabra2*. Quantifications were done in the cell body and in the proximal domain (*i.e.*, the portion located in the GCL) of the apical dendrite (Fig. 1*C-E*). Two-way ANOVA revealed a significant effect of genotype and a significant interaction between time and genotype in both regions (Table 3). In WT mice, the density of α2-subunit-positive perisomatic clusters increased significantly from 7 to 90 dpi, whereas that of dendritic clusters remained constant during the same period (one-way ANOVA, cell body $F_{3,8} = 5.752$, $P = 0.0214$; apical dendrite $F_{3,8} = 3.438$, $P = 0.07$). Surprisingly, in α2-FL mice α2-subunit-positive clusters were still detectable on eGFP$^+$ cells at 7 and 14 dpi. However, a strong decrease was observed at 30 and 90 dpi in both the somatic and dendritic compartments (Fig. 1*E*; one-way ANOVA, cell body: $F_{3,8} = 5.677$, $P = 0.022$; apical dendrite: $F_{3,8} = 7.879$, $P = 0.009$). These results suggest that *Gabra2* is expressed early in adult-born GCs and that following Cre-mediated inactivation, the loss of α2-subunit is a protracted process that takes place during the early phase of GC maturation.

We next verified whether the α3 subunit, which is also expressed in GCs (Fritschy and Mohler, 1995), is upregulated after *Gabra2* inactivation (Fig. 1*D, F*). At 90 dpi, there was no difference in α3-subunit cluster density in GCs of α2-FL and WT mice (cell body: $t_3 = 1.147$, $P = 0.315$; apical dendrite: $t_3 = 0.284$, $P = 0.790$), suggesting that deletion of the α2-subunit is not compensated by increased expression of the α3-subunit.

We then analyzed how deletion of the α2-subunit affects GABAergic innervation of GCs. We first quantified postsynaptic gephyrin clusters (Fig. 1*G-H*) and found a significant

decrease in GCs of α2-FL mice, in parallel with the depletion of the α2-subunit (one-way ANOVA, cell body: $F_{3,8} = 6.735$, $P = 0.014$; apical dendrite: $F_{3,8} = 7.472$, $P = 0.01$; see Table 3 for overall statistics). In contrast, there was no difference, at any time-point, in the number of $GAD65^+$ terminals impinging onto the cell body and the apical dendrite of $eGFP^+$ GCs (Fig. 1*I-J*; Table 3). These data indicate that GABAergic innervation of GCs is maintained after deletion of the α2-subunit despite the disruption of the postsynaptic gephyrin scaffold.

Conditional deletion of *Gabra2* causes delayed decrease of GABAergic currents in adult-born granule cells

We performed whole-cell patch-clamp recordings on acute OB slices to investigate the functional consequence of *Gabra2* inactivation. Using a focal electrical stimulation delivered in the GCL (Fig. 2*A*), we recorded evoked inhibitory post-synaptic currents (eIPSCs) in adult-born GCs (Fig. 2*B*). Two-way ANOVA revealed a significant effect of time and genotype and a significant interaction between these factors (see Tables 4 and 5*A* for values and statistics). In cells from WT mice, we observed a significant increase in the amplitude of eIPSCs over time, from 7 to 90 dpi (one-way ANOVA, $P = 0.002$), consistent with the progressive increase in α2-subunit and gephyrin clusters described above. However, the amplitude of eIPSCs remained constant in α2-FL mice, leading to a five-fold difference at 90 dpi when compared to WT (Fig. 2*C* and Table 5*A*). We next tested the consequences of ablation of the α2-subunit on the physiological properties of spontaneous IPSCs (sIPSCs) (Fig. 2*D-H* and Table 5*A*). While there was no change over time in either genotype (two-way ANOVA, Table 4), the amplitude of sIPSCs was significantly lower in α2-FL cells than in WT at all *time-point*s after 14 dpi (Fig. 2*E* and Table 5*A*). Concomitantly, the sIPSC frequency increased over time in WT (one-way ANOVA, $P = 0.031$) reflecting the progressive increase in the number of functional synapses, but remained constant in mutant GCs (Fig. 2*F*). The decay time constants were longer in mutant cells (Fig. 2*D*, *G*), but the rise times remained unchanged (Fig. 2*H*) (Tables 4 and 5*A*). In contrast to these dramatic changes, when intrinsic membrane properties were analyzed, we found no genotype effect on the membrane capacitance, input membrane resistance, and the Na^+ current density (Table 6). Thus, ablation of the α2-subunit led to a marked reduction in the functional properties of GABAergic synapses without changing the electrophysiological intrinsic properties of newborn GCs. Collectively, these results are consistent with the immunohistochemical data showing an increased number of GABAergic synapses during the morphological maturation of GCs, a process that is dramatically altered in

mutant cells. Inactivation of *Gabra2* leads to the formation of adult-born GCs receiving fewer GABAergic inputs characterized by low amplitude and slow decay time constants. These alterations appear at about 14 dpi and become even more apparent at later time-points.

Granule cell dendritic morphology is affected after *Gabra2* inactivation

To determine whether the reduced afferent GABAergic signaling caused by conditional deletion of *Gabra2* has an influence on the survival of newborn GCs, we determined the density of $eGFP^+$ cell at different time-points after viral injection. We found that cell density remained constant did not differ between the two genotypes (*i.e.*, at 90 dpi WT: 1,350 ± 50 cells/mm^2; α2-FL: 1,200 ± 27 cells/mm^2; unpaired *t*-test, $P = 0.676$), indicating that deletion of the α2-subunit does not affect GC survival. However, double-labeling for eGFP and doublecortin (Dcx) revealed that mutant GCs have a prolonged expression of Dcx compared to control (30 dpi: 7.1 ± 0.9 % and 19 ± 1.8 % in WT and α2-FL mice, respectively; n = 688 and 394 cells; 90 dpi: 5 ± 0.1 % and 11.1 ± 0.7 % in WT and α2-FL mice; n = 710 and 564 cells). These results indicate that adult-born GCs lacking α2-$GABA_A$Rs exhibit impaired structural maturation compared to the WT counterpart.

We then asked whether the reduction in GABAergic inputs could alter the dendritic arborization of newborn GCs. As expected for maturing cells, Sholl analysis of WT control cells revealed a progressive development of the dendritic tree, in particular in the distal portion starting around 100 μm away from the cell body (see Fig. 3*A*). Calculating the total area under the curve (AUC; Fig. 3*A*), we observed a 44% increase between 7 and 30 dpi, followed by a significant reduction at 90 dpi (one-way ANOVA, $F_{3,8} = 30.07$, $P = 0.0001$). This suggests that the apical dendrite undergoes a prominent remodeling after an initial period of exuberant growth. In α2-FL mice, dendritic development beyond 14 dpi was altered compared to WT (Fig. 3*B*). Sholl analysis revealed a slow increase of the AUC between 14 and 90 dpi, which reached significance only at the later time-point (Table 7*A*). Likewise, analysis of the total dendritic length and the number of terminal branches revealed significant effects of genotype and time, as well as a strong interaction between both factors (two-way ANOVA; Table 7*B*). While these parameters increased significantly at 30 and 90 dpi in WT, there were only limited changes in GCs from α2-FL mice (Fig. 3*C-E*). Therefore, dendritic growth of adult-born GCs is severely impaired upon ablation of α2-$GABA_A$Rs.

***Gabra2* inactivation causes rearrangements of glutamatergic synapses**

To further substantiate the role of α2-$GABA_A$Rs in modulating GC differentiation and synaptic integration, we investigated whether excitatory synapses also change following *Gabra2* inactivation. Quantification of spine density in the GCL and EPL (Fig. 4*A-D*) revealed highly significant effects of time and genotype, as well as a strong interaction between these factors (two-way ANOVA, Table 7*B*). In WT mice, spine density increased from 7 to 14 dpi, followed by stabilization and a decrease between 30 and 90 dpi (Fig. 4*B*, *D*). This transient peak in spine density is consistent with previous investigations (Whitman and Greer, 2007) and may be related to the critical window of activity-dependent plasticity that characterizes GC development (Kelsch et al., 2009; Nissant et al., 2009). A similar trend was seen in α2-FL mice, but the peak in spine density between 14 and 30 dpi was much less pronounced (Fig. 4*B*, *D*). Despite these changes in spine density, there were no obvious alterations in spine morphology, and spine neck length and head area were similar in α2-FL and WT mice (data not shown). These data indicate that the α2-subunit is necessary for the formation of an exuberant number of spines, which are then pruned after 30 dpi.

We used antibodies against PSD95 to understand whether the lower spine density seen in mutant GCs is accompanied by a rearrangement of glutamatergic synapses (Fig. 4*E-F*). While the number of PSD95 clusters located in spines was reduced in GCs of α2-FL mice, reflecting spine deficit (Fig. 4*E*, $t_3 = 3.349$; $P = 0.029$ at 90 dpi), the density of PSD95 clusters on the dendritic shaft was significantly higher than in WT (Fig. 4*E*, $t_3 = 3.464$; $P = 0.026$). These observations suggest that deletion of α2-$GABA_A$Rs in GCs causes glutamatergic synapses to persist on dendritic shafts. To confirm this, we performed preembedding immuno-electron microscopy for eGFP and gephyrin on α2-FL mice at 90 dpi. This analysis revealed that mitral/tufted cell dendrites establish reciprocal synapses with $eGFP^+$ profiles that lack the typical morphology of GC spines, supporting the idea that the reduction of spine density in mutant GCs is concurrent with the persistence of excitatory synapses on the dendritic shaft (Fig. 4*G-H*).

Finally, we analyzed the properties of glutamatergic synapses in mutated GCs. For this, spontaneous excitatory postsynaptic currents (sEPSCs) were recorded during a 5-min baseline period. Analysis of their frequency revealed a similar profile as spine density, with significant effects of time and genotype (see Table 4 and 6*B* for values and statistics). At 14 and 30 dpi, α2-FL cells had a significant lower sEPSCs frequency compared to WT GCs (one-way ANOVA, $P = 0.021$; Fig. 4*I-J*) but their amplitude (one-way ANOVA, $P = 0.583$; Fig. 4*K*), decay kinetics (one-way ANOVA, $P = 0.267$; Fig. 4*L*) and rise time (one-way

ANOVA, $P = 0.08$; not shown) remained unchanged. Thus, we conclude that GCs lacking α2-$GABA_A$Rs develop a reduced number of functionally unchanged glutamatergic synapses. The reduced sEPSC frequency in mutant cells correlates well with the overall decrease of PSD95 clusters.

Gabra2 inactivation occludes the effect of sensory deprivation on spine density in granule cells

We examined the putative role of α2-$GABA_A$Rs in activity-dependent regulation of structural plasticity by challenging the degree of sensory inputs to the OB circuit. We used both olfactory enrichment and dichlobenil-mediated sensory deprivation to study the adaptability of adult-born GCs to their novel neuronal environment. Mice were exposed to the enriched environment or injected with dichlobenil at 7 dpi and were sacrificed at 30 dpi (Fig. 5*A*). In WT mice, odor enrichment caused a small increase in spine density that did not reach statistical significance, whereas olfactory deprivation caused a marked reduction in the density of spines (Fig. 5*B-C*) (one-way ANOVA, $P = 0.002$). In contrast, in α2-FL mice neither enrichment nor sensory deafferentation caused significant changes in the density of spines. This indicates that inhibitory synaptic transmission mediated by α2-$GABA_A$Rs is required for structural adaptations of newborn GCs triggered by sensory enrichment or deprivation during the phase of dendritic/spine exuberance.

Effects of early ablation of *Gabra2* in progenitor neural cells

In the α2-FL model, deletion of the α2-subunit is complete only after GCs have reached the OB and started to establish synaptic connections within the pre-existing network. We devised a complementary approach to inactivate *Gabra2* in neural precursor cells of adult mice, prior to their final mitotic division and migration to the OB. This was achieved by crossing α2-FL mice with mice expressing an inducible form of Cre (Cre-ERT2) under the control of the GLAST promoter (Mori et al., 2006). At the age of 8 weeks mice were treated systemically with tamoxifen or vehicle (hereafter called Tam and Oil, respectively); four weeks later, they were injected stereotaxically with a lentiviral vector encoding eGFP (Fig. 6*A*). Adult-born GCs were investigated morphologically and functionally at 7 dpi and 90 dpi.

Quantification of the number of $eGFP^+$ cells in the GCL showed no difference in mice injected with tamoxifen or oil neither at 7 dpi (Oil: 527 ± 159 cells/mm^2 and Tam: 414 ± 36 cells/mm^2, unpaired t-test, $t_4 = 0.694$, p= 0.525), nor at 90 dpi (Oil: 780 ± 27 cells/mm^2; Tam:

647 ± 143 cells/mm^2; un-paired t-test, $t_4 = 0.915$ $P = 0.412$). We then analyzed the density of α2-subunit clusters on the cell body and the apical dendrite of eGFP$^+$ cells. We found a strong decrease in cluster density in Tam-injected mice compared to the control group already at 7dpi (cell body: $t_4 = 6.119$, $P = 0.0036$; apical dendrite: $t_4 = 15.01$, $P < 0.0001$) (Fig. 6*B-C*). Similarly, we observed a decreased density of gephyrin clusters in the proximal portion of the apical dendrite of Tam mice (Oil: 0.169 ± 0.016 clusters/μm; Tam: 0.080 ± 0.016 clusters/μm; $t_4 = 3.871$, $P = 0.018$). Triple-immunofluorescence staining confirmed that these remaining gephyrin clusters were colocalized the α3-subunit (not shown). Accordingly, the density of α3/gephyrin clusters was similar in both groups (Fig. 6*D*) in the cell body ($t_4 = 1.186$, $P = 0.30$) and in the apical dendrite ($t_4 = 0.381$, $P = 0.72$), indicating that no compensation occurs, like in α2-FL mice.

We then investigated whether this early deletion of the α2-subunit impairs dendritic development similar to the situation in α2-FL mice. eGFP$^+$ cells in Tam-injected mice showed reduced dendritic branching (Fig. 6*E*), with the number of terminal branches being significantly lower already at 7 dpi (Fig. 6*F*; $t_4 = 5.712$, $P = 0.0046$), a defect that persisted until 90 dpi (Fig. 6*F*; $t_4 = 5.129$, $P = 0.0068$). This reduction was also reflected in the Sholl analysis made at 90 dpi, revealing significantly reduced AUC (Fig. 6*G*; Oil: 366 ± 7.7; Tam: 289 ± 11.8; $t_4 = 6.895$, $P = 0.002$), particularly at the 100-250 μm interval from the cell body. Spine density was also significantly decreased in Tam-treated mice at 7 dpi (Fig. 6*H*) and this defect persisted at 90 dpi (Fig. 6*I-J*; 7 dpi: $t_4 = 11.44$, $P = 0.0003$; 90 dpi: $t_4 = 7.741$, $P = 0.0015$). The reduced spine density was accompanied by a decreased number of PSD95 clusters in spines (Fig. 6*J-K*; t_4=12.02, $P = 0.0003$). However, in contrast with α2-FL mice, we did not observe an increase in the density of PSD95 clusters along dendritic profiles. These data indicate that early depletion of the α2-subunit accelerates developmental alterations in newborn GCs but eventually results in structural defects that largely overlap with those seen in α2-FL mice.

Discussion

In this study, we show that functional α2-$GABA_A$Rs are required for proper structural development of adult-born GCs and for the onset of its sensory-dependent regulation. Major deficits of GCs lacking α2-$GABA_A$Rs include absence of spine/dendrite overproduction around 30 dpi, persistence of glutamatergic synapses on their dendritic shaft, and inability to adjust their morphology to sensory enrichment or deprivation. Similar observations were made when *Gabra2* was inactivated in neural stem cells or in migrating neuroblasts. Thus, our work demonstrates that GABAergic synaptic inhibition is an important determinant of the activity-dependent regulation of synaptic integration of adult-generated OB neurons.

Specificity and efficiency of α2-subunit deletion of $GABA_A$Rs

Adult-born GCs express $GABA_A$Rs early in development and thus are responsive to GABAergic signals already in the neurogenic zone and in the RMS (Platel et al., 2008). Sixteen $GABA_A$R subunits are expressed in a time- and location-specific manner in the developing and adult brain (Laurie et al., 1992; Fritschy and Brünig, 2003). In particular, because $GABA_A$R subtypes have unique functional properties, their interaction with environmental cues may differentially regulate distinct steps of adult neurogenesis (Duveau et al., 2011). In the SVZ-OB system, multiple $GABA_A$R subunits have been detected in neonatal neuroblasts (Stewart et al., 2002) and PSA-NCAM-positive progenitors derived from neurospheres (Nguyen et al., 2003). Adult GCs most likely express distinct $GABA_A$R subtypes mediating tonic and phasic inhibition. Here, we focused on α2-$GABA_A$Rs, which represent the majority of postsynaptic receptors in GCs and are absent from MCs and tufted cells (Panzanelli et al., 2009). We silenced these receptors by two means. We injected a CRE-IRES-eGFP-encoding lentivirus into the RMS of adult α2-FL mice, or we employed eGFP-encoding lentivirus injected into Glast*::*creERT2$^{+/-}$ mice previously treated with tamoxifen. We found that disappearance of the α2-subunit requires at least three weeks after injection of the lentiviral vector (Fig. 1). Therefore, in the first model (α2-FL mice) α2-$GABA_A$Rs were removed only after newly-formed GCs had already reached the OB, thus avoiding potential compensatory mechanisms that could take place during earlier development. In the second approach, α2-$GABA_A$Rs were invalidated already in adult neural stem cells (*i.e.*, Glast-expressing cells) before their final neuronal commitment. Remarkably, most of the observations made in the first model were validated by the second approach, thus ruling out any potential bias due to early GABAergic signaling that was preserved in developing GCs of

α2-FL mice. It is also worth noting that in both genetic models, the dramatic reduction of α2-$GABA_A$Rs did not induce compensatory up-regulation of the α3-subunit, resulting in a severe down-regulation of synaptic GABAergic transmission. As expected, however, the strongly decreased expression of $GABA_A$Rs correlated with reduced amplitude and frequency of spontaneous synaptic GABAergic events. In addition, because the rise time of sIPSCs was unchanged after deleting the α2-subunit, we conclude that the reduction of GABAergic inputs is rather homogeneous between the somatic and dendritic compartments. The few currents that remain in GCs of α2-FL mice have a kinetic profile consistent with $GABA_A$Rs containing the α3 subunit (Schofield et al., 2009). Notably, these small and slow currents were not sufficient to rescue the maturation of newborn GCs.

Despite these postsynaptic alterations and the loss of gephyrin clusters caused by *Gabra2* inactivation, GABAergic terminals remained remarkably unchanged. This finding illustrates the robustness of presynaptic GABAergic terminals when the postsynaptic site is challenged, in line with observations make in α2-KO mice (Panzanelli et al., 2011). Finally, in both experimental settings, *Gabra2* inactivation did not affect GC survival (as assessed by quantifying the number of $eGFP^+$ cells in the GCL), indicating that functional GABAergic synapses are dispensable for long-term survival of adult-born GCs.

Impaired morphological maturation in granule cells receiving fewer GABAergic inputs

GABA is considered a key actor at early stages of adult neurogenesis. In the SVZ, it reduces the number of proliferative neural stem cells via tonic activation of $GABA_A$Rs (Liu et al., 2005). Similarly, GABAergic signaling controls neuroblast migration in the RMS via paracrine effects (Bolteus and Bordey, 2004; Ge et al., 2006; Platel et al., 2008). These early functions demonstrate that GABA spill-over might provide important information to neural stem cells and migrating progenitors about the size of the population of neuroblasts already formed (Platel et al., 2007). However, while these previous studies indicate that GABA controls these stages of cell development, the function of GABAergic signaling on the ensuing maturation of GCs has remained rather elusive.

We show here that reducing synaptic transmission mediated by α2-$GABA_A$Rs in developing GCs has detrimental effects on their structural maturation. Specifically, postsynaptic currents mediated by α2-$GABA_A$R are required to control dendritic growth and spine formation after GCs have reached their final destination in the OB. During their maturation, adult-born GCs receive synaptic inputs from several distinct glutamatergic and GABAergic neurons (Whitman and Greer, 2009; Kelsch et al., 2010; Nissant and Pallotto,

2011). Furthermore, GC maturation is characterized by an initial overproduction of spines and glutamatergic synapses, followed by a phase of synaptic pruning ((Whitman and Greer, 2007) and the present study), likely corresponding to a phase of maturation during which synapses are refined by activity-dependent mechanisms. In striking contrast, in newborn GCs lacking the α2-subunit, this window of increased plasticity appears to be suppressed, as dendritic length, spine density, and glutamatergic synapses remained rather constant during the entire developmental period examined. Therefore, functional α2-$GABA_A$Rs at afferent GABAergic synapses are essential for proper synaptic integration of adult-born GCs. This conclusion is in agreement with another study showing that blockade of $GABA_A$Rs triggered a rapid stabilization of new dendritic segments in acute OB slices (Gascon et al., 2006). Further evidence for a developmental "freezing" in the absence of α2-$GABA_A$Rs was provided here by extended expression of Dcx in a subset of cells and the persistence of glutamatergic synapses on dendritic shafts of mutant GCs up to 90 dpi. We have shown previously in WT mice that dendro-dendritic synapses initially form on the shaft of GC dendrites, before being transferred to spines (Panzanelli et al., 2009). This morphological rearrangement is disrupted in mutant GCs, most likely reflecting an intrinsic deficit in spine formation.

The mechanisms by which $GABA_A$R activation contributes to regulate dendritic development and glutamatergic synaptogenesis remain to be determined. In the dentate gyrus, GABA supports neuronal maturation by increasing the expression of transcription factors necessary for neuronal differentiation (Tozuka et al., 2005). The demonstration that local calcium signaling plays a key role for selecting among potential synaptic partners (Lohmann and Bonhoeffer, 2008) might be related with our observations. Similarly, our data are in line with work in the hippocampus according to which GABA regulates dendritic arborization and synapse formation in adult-generated neurons (Ge et al., 2006), possibly via the control of CREB-dependent transcriptional events (Merz et al., 2011). In keeping with the evidence that GABA-mediated depolarization regulates synaptic development of young neurons during development (Wang and Kriegstein, 2008), our results suggest that activation of postsynaptic GABAergic signaling is linked to signaling cascades controlling multiple aspects of neuronal maturation.

The present results reveal apparent differences in the role of α2-$GABA_A$Rs during maturation of adult-born GCs in the OB and in the dentate gyrus (Duveau et al., 2011). In the latter study, analysis of both global *Gabra2* inactivation and single-cell deletion with Cre-expressing viruses demonstrated normal initial dendritic growth and spine formation,

followed by excessive dendritic pruning in 4-6 week-old cells. This dendritic pruning could be prevented by pharmacologically reducing glutamatergic synaptogenesis, suggesting that it represented a homeostatic mechanism to preserve inhibitory-excitatory balance in newborn neurons and/or it could be a consequence of activity-dependent dendritic development. This relatively mild phenotype compared to the one observed here in OB GCs likely reflects the fact that α1-$GABA_A$Rs are largely preserved in the dentate gyrus upon *Gabra2* inactivation, implying a less dramatic impairment of postsynaptic GABAergic function. Nevertheless, these studies collectively indicate that functional α2-$GABA_A$Rs are required for normal structural development and functional maturation of adult-born neurons in the brain.

Absence of activity-dependent regulation in granule cells lacking proper GABAergic inhibition

Our study supports an important role of GABAergic inhibition for the activity-dependent selection of synaptic connectivity that occurs during a critical window of GC development, and links this observation to previous studies showing that sensory stimulation is an important determinant of the fate of adult-generated neurons. Because the OB circuit is located only at one synaptic relay from the external world, we sought to examine the potential role for GABA in mediating circuit remodeling induced by sensory experience (Saghatelyan et al., 2005). When challenging the degree of sensory inputs to the OB, we found that neither sensory enrichment nor sensory deafferentation caused significant changes in spine density in α2-FL mice. This observation indicates that GABAergic synaptic transmission mediated by α2-$GABA_A$Rs is required for structural adaptations of adult-born GCs to sensory challenges during the phase of dendritic/spine exuberance. Further studies will have to explore whether the α2-$GABA_A$R's effects on activity-dependent mechanisms depend on the depolarizing or hyperpolarizing action of GABA.

In summary, deletion of α2-$GABA_A$Rs in newborn GCs caused a profound reduction in synaptic inhibition and impaired their maturation and synaptic integration. These effects occurred whether the α2-subunit was removed at early or late stages of GC development. Notably, we found that even though the excitatory/inhibitory balance remained constant when deleting synaptic $GABA_A$Rs, the regulation brought into play by sensory experience was lacking. With further technological advances and new tools applied to the study of adult neurogenesis, we will undoubtedly decipher the mechanism by which such simple molecule can have so many crucial effects.

References

Altman J (1969) Autoradiographic and histological studies of postnatal neurogenesis. IV. Cell proliferation and migration in the anterior forebrain, with special reference to persisting neurogenesis in the olfactory bulb. J Comp Neurol 137:433-458.

Alvarez-Buylla A, Garcia-Verdugo JM (2002) Neurogenesis in adult subventricular zone. J Neurosci 22:629-634.

Bolteus AJ, Bordey A (2004) GABA release and uptake regulate neuronal precursor migration in the postnatal subventricular zone. J Neurosci 24:7623-7631.

Chang YC, Gottlieb DM (1988) Characterization of the proteins purified with monoclonal antibodies to glutamic acid decarboxylase. J Neurosci 8:2123-2130.

Duveau V, Laustela S, Barth L, Gianolini *F*, Vogt KE, Keist R, Chandra D, Homanics GE, Rudolph U, Fritschy JM (2011) Spatiotemporal specificity of $GABA_A$ receptor-mediated regulation of adult hippocampal neurogenesis. Eur J Neurosci 34:362-373.

Fritschy JM, Mohler H (1995) $GABA_A$-receptor heterogeneity in the adult rat brain: differential regional and cellular distribution of seven major subunits. J Comp Neurol 359:154-194.

Fritschy JM, Brünig I (2003) Formation and plasticity of GABAergic synapses: physiological mechanisms and pathophysiological implications. Pharmacol Ther 98:299-323.

Gascon E, Dayer AG, Sauvain MO, Potter G, Jenny B, De Roo M, Zgraggen E, Demaurex N, Muller D, Kiss JZ (2006) GABA regulates dendritic growth by stabilizing lamellipodia in newly generated interneurons of the olfactory bulb. J Neurosci 26:12956-12966.

Ge S, Goh EL, Sailor KA, Kitabatake Y, Ming GL, Song H (2006) GABA regulates synaptic integration of newly generated neurons in the adult brain. Nature 439:589-593.

Grubb MS, Nissant A, Murray K, Lledo PM (2008) Functional maturation of the first synapse in olfaction: development and adult neurogenesis. J Neurosci 28:2919-2932.

Holderith NB, Shigemoto R, Nusser Z (2003) Cell type-dependent expression of HCN1 in the main olfactory bulb. Eur J Neurosci 18:344-354.

Katagiri H, Pallotto M, Nissant A, Murray K, Sassoe-Pognetto M, Lledo PM (2011) Dynamic development of the first synapse umpinging on adult-born olfactory neurons. Neural Syst Circuits 1:6.

Kelsch W, Lin CW, Lois C (2008) Sequential development of synapses in dendritic domains during adult neurogenesis. Proc Natl Acad Sci U S A 105:16803-16808.

Kelsch W, Sim S, Lois C (2010) Watching synaptogenesis in the adult brain. Annu Rev Neurosci 33:131-149.

Kelsch W, Lin C, Mosley C, Lois C (2009) A critical period for activity-dependent synaptic development during olfactory bulb adult neurogenesis. J Neurosci 29:11852-11858.

Kempermann G, Jessberger S, Steiner B, Kronenberg G (2004) Milestones of neuronal development in the adult hippocampus. Trends Neurosci 27:447-452.

Kollo M, Holderith N, Antal M, Nusser Z (2008) Unique clustering of A-type potassium channels on different cell types of the main olfactory bulb. Eur J Neurosci 27:1686-1699.

Laurie DJ, Wisden W, Seeburg PH (1992) The distribution of thirteen $GABA_A$ receptor subunit mRNAs in the rat brain. III. Embryonic and postnatal development. J Neurosci 12:4151-4172.

Liu X, Wang Q, Haydar TF, Bordey A (2005) Nonsynaptic GABA signaling in postnatal subventricular zone controls proliferation on GFAP-expressing progenitors. Nature Neurosci:1179-1187.

Lledo PM, Alonso A, Grubb MS (2006) Adult neurogenesis and functional plasticity in neuronal circuits. Nat Rev Neurosci 7:179-193.

Lohmann C, Bonhoeffer T (2008) A role for local calcium signaling in rapid synaptic partner selection by dendritic filopodia. Neuron 59:253-260.

Merz K, Herold S, Lie DC (2011) CREB in adult neurogenesis--master and partner in the development of adult-born neurons? Eur J Neurosci 33:1078-1086.

Ming GL, Song H (2011) Adult neurogenesis in the mammalian brain: significant answers and significant questions. Neuron 70:687-702.

Mori T, Tanaka K, Buffo A, Wurst W, Kühn R, Götz M (2006) Inducible gene deletion in astroglia and radial glia--a valuable tool for functional and lineage analysis. Glia 54:21-34.

Nguyen L, Malgrange B, Breuskin I, Bettendorff L, Moonen G, Belachew S, Rigo JM (2003) Autocrine/paracrine activation of the $GABA_A$ receptor inhibits the proliferation of neurogenic polysialylated neural cell adhesion molecule-positive ($PSA\text{-}NCAM^+$) precursor cells from postnatal striatum. J Neurosci 23:3278-3294.

Nissant A, Pallotto M (2011) Integration and maturation of newborn neurons in the adult olfactory bulb--from synapses to function. Eur J Neurosci 33:1069-1077.

Nissant A, Bardy C, Katagiri H, Murray K, Lledo PM (2009) Adult neurogenesis promotes synaptic plasticity in the olfactory bulb. Nature Neurosci 12:728-730.

Panzanelli P, Bardy C, Nissant A, Pallotto M, Sassoè-Pognetto M, Lledo P, Fritschy J (2009) Early synapse formation in developing interneurons of the adult olfactory bulb. J Neroscience 29:15039-15052.

Panzanelli P, Gunn B, Schlatter M, Benke D, Tyagarajan S, Scheiffele P, Belelli D, Lambert J, Rudolph U, Fritschy J (2011) Distinct mechanisms regulate GABAA receptor and gephyrin clustering at perisomatic and axo-axonic synapses on CA1 pyramidal cells. J Physiol 589:4959-4980.

Platel JC, Lacar B, Bordey A (2007) GABA and glutamate signaling: homeostatic control of adult forebrain neurogenesis. J Mol Histol 38:602-610.

Platel JC, Dave KA, Bordey A (2008) Control of neuroblast production and migration by converging GABA and glutamate signals in the postnatal forebrain. J Physiol 586:3739-3743.

Rochefort C, Gheusi G, Vincent JD, Lledo PM (2002) Enriched odor exposure increases the number of newborn neurons in the adult olfactory bulb and improves odor memory. J Neurosci 22:2679-2689.

Saghatelyan A, Roux P, Migliore M, Rochefort C, Desmaisons D, Charneau P, Shepherd GM, Lledo PM (2005) Activity-dependent adjustments of the inhibitory network in the olfactory bulb following early postnatal deprivation. Neuron 46:103-116.

Schneider Gasser EM, Straub CJ, Panzanelli P, Weinmann O, Sassoè-Pognetto M, Fritschy JM (2006) Immunofluorescence in brain sections: simultaneous detection of presynaptic and postsynaptic proteins in identified neurons. Nature Protocols 1:1887-1897.

Schofield CM, Kleiman-Weiner M, Rudolph U, Huguenard JR (2009) A gain in $GABA_A$ receptor synaptic strength in thalamus reduces oscillatory activity and absence seizures. Proc Natl Acad Sci U S A 106:7630-7635.

Shepherd GM, Chen WR, Willhite D, Migliore M, Greer CA (2007) The olfactory granule cell: from classical enigma to central role in olfactory processing. Brain Res Rev 55:373-382.

Stewart R, Hoge G, Zigova T, Luskin M (2002) Neural progenitor cells of the neonatal rat anterior subventricular zone express functional $GABA_A$ receptors. J Neurobiol 50:305-322.

Stone D, Grillo M, Margolis *F*, Joh T, Baker H (1991) Differential effect of functional olfactory bulb deafferentation on tyrosine hydroxylase and glutamic acid

decarboxylase messenger RNA levels in rodent juxtaglomerular neurons. J Comp Neurol 311:223-233.

Tozuka Y, Fukuda S, Namba T, Seki T, Hisatsune T (2005) GABAergic excitation promotes neuronal differentiation in adult hippocampal progenitor cells. Neuron 47:803-815.

Vedin V, Slotnick B, Berghard A (2004) Zonal ablation of the olfactory sensory neuroepithelium of the mouse: effects on odorant detection. Eur J Neurosci 20:1858-1864.

Waclaw RR, Allen ZJ, Bell SM, Erdélyi *F*, Szabó G, Potter SS, Campbell K (2006) The zinc finger transcription factor Sp8 regulates the generation and diversity of olfactory bulb interneurons. Neuron 49:503-516.

Wang DD, Kriegstein AR (2008) GABA regulates excitatory synapse formation in the neocortex via NMDA receptor activation. J Neurosci 28:5547-5558.

Whitman MC, Greer CA (2007) Synaptic integration of adult-generated olfactory bulb granule cells: basal axodendritic centrifugal input precedes apical dendrodendritic local circuits. J Neurosci 27:9951-9961.

Whitman MC, Greer CA (2009) Adult neurogenesis and the olfactory system. Prog Neurobiol 89:162-175.

Witschi R, Punnakkal P, Paul J, Walczak JS, Cervero *F*, Fritschy JM, Kuner R, Keist R, Rudolph U, Zeilhofer HU (2011) Presynaptic α2-$GABA_A$ receptors in primary afferent depolarization and spinal pain control. J Neurosci 31:8134-8142.

Yamaguchi M, Mori K (2005) Critical period for sensory experience-dependent survival of newly generated granule cells in the adult mouse olfactory bulb. Proc Natl Acad Sci U S A 102:9697-9702.

Figure Legends

Figure 1: Effects of CRE-mediated deletion of *Gabra2* gene in adult-born granule cells. **A)** Schematic diagram of the experimental approach to label adult-born GCs by stereotaxic injection of a lentiviral vector expressing CRE recombinase and eGFP into the RMS. Infected cells are readily recognized by eGFP labeling. **B)** Schematic localization of the markers analyzed by immunohistochemistry at GABAergic synapses made on adult-born GCs. **C)** Images from confocal laser scanning microscopy depicting the presence of α2-subunit immunoreactive clusters (red) in $eGFP^+$ cells of WT and α2-FL mice after 90 dpi, confirmed by colocalization analysis (yellow; arrowheads). Note the almost complete disappearance of α2-subunit clusters in adult-born cells of α2-FL mice at this stage. Each image represents a 3-D projection of a stack of confocal layers spaced 0.35 µm, shown in the three Cartesian planes. **D)** Images depicting the presence of α3-subunit clusters (red) in $eGFP^+$ cells of WT and α2-FL mice after 90 dpi, as confirmed by colocalization analysis (yellow, arrowheads). **E-*F*)** Quantification of α2- and α3-subunit clusters (mean ± SEM) in the cell body and apical dendrite of adult-born GCs in WT and α2-FL mice. **G)** Images of gephyrin clusters (red) in $eGFP^+$ cells of WT and in α2-FL mice after 90 dpi, as confirmed by colocalization analysis (yellow; arrowheads). **H)** Quantification of gephyrin clusters (mean ± SEM) showing the decreased gephyrin cluster density in cell body and in the apical dendrite in mutant cells at 30-90 dpi. **I)** Images depicting the presence of GAD65-immunoreactive puncta apposed to $eGFP^+$ cells (yellow, arrowheads) after 90 dpi in both genotypes. **J)** Quantification of GAD65 puncta, representing putative synaptic input, onto the cell body and apical dendrite of adult-born GCs (mean ± SEM). No difference was observed at any *time-point*. *$P < 0.05$, one-way ANOVA with post-test (see Table 3 for statistical analyses). Scale bars: 10 µm.

Figure 2: Reduction of GABAergic currents in newborn GCs from α2-FL mice. Electrophysiological properties of $eGFP^+$ GCs were assessed by whole-cell patch-clamp recordings. **A)** Recording configuration. EPL: external plexiform layer, GCL: granule cell layer, GC granule cell, Rec: recording electrode, Stim: stimulation electrode located in the GCL to elicit IPSCs (glass pipette). **B)** Examples of evoked inhibitory post-synaptic currents (eIPSCs) recorded at $V_c = 0$ mV at 14 dpi. Representative traces were averaged from >20 recorded IPSCs; calibration bars: 20 ms, 25 pA. **C)** Histograms of eIPSC amplitude (pA; mean ± SD) for WT and α2-FL cells. **D)** Examples of spontaneous IPSCs (sIPSCs) recorded

from a WT cell (grey) and an α2-FL cell (red) at 30 dpi (V_c= 0 mV; calibration bars: 50 ms, 10 pA). In the right panel, normalized sIPSC amplitudes are displayed to illustrate their relative kinetics. **E-*F*)** Histograms of the frequency and amplitude of sIPSCs in WT and α2-FL cells (mean ± SD). **G-H)** Histograms of sIPSC decay time constant (Tau_{fast} derived from double exponential fitting) and rise time (measured from 20 to 80% of peak amplitude). See Tables 4 and 5*A* for statistical analysis (* P < 0.05; ** P < 0.01; ***P < 0.001).

Figure 3: Morphometric analysis of apical dendrite arborization in newborn GCs of WT and α2-FL mice. A) Quantification by Sholl analysis of apical dendrites in $eGFP^+$ cells of WT mice. The number of intersections between $eGFP^+$ dendritic segments and virtual concentric lines centered on the soma and spaced by 10 μm is displayed graphically. Each curve represents the situation at individual time-points after virus injection. For comparison between different time-points, the "area under the curve" (AUC) was calculated and analyzed statistically by one-way ANOVA with post-hoc tests (*P < 0.05, **P < 0.01, ***P < 0.001). **B)** Sholl analysis comparison between WT (grey line) and α2-FL mice (red line) illustrating the reduction in dendritic complexity in newborn GCs from α2-FL mice. Most differences occur in the EPL (> 100 μm from the soma) and are most pronounced at 30 dpi. For statistical comparison between genotypes, the corresponding AUC was calculated in each graph (see Table 7*A* for mean values and statistical results). **C)** Representative drawings of $eGFP^+$ cells in WT and α2-FL mice used for Sholl analysis at 14 and 90 dpi. **D-E)** Histograms of the total apical dendrite length and number of terminal branches (mean ± SEM) in WT and α2-FL mice (one-way ANOVA with post-tests; see Table 7*B* for statistical analysis; *p < 0.05).

Figure 4: Altered excitatory inputs in newborn GCs from α2-FL mice. A, C) Representative images of dendritic spines on the apical dendrites of $eGFP^+$ cells of WT and α2-FL mice in the GCL (A) and EPL (C) at 30 and 90 dpi. **B, D)** Quantification of spine density (mean ± SEM) on apical dendrites in the GCL (B) and EPL (D); one-way ANOVA with post-tests (*P < 0.05; see Table 7*B* for general statistical analysis). **E)** Quantification of PSD95 clusters colocalized with eGFP on the spines and the shaft of apical dendrite at 90 dpi (mean ± SEM; *P<0.05, two-tailed Student's *t*-test). ***F*)** Images (3-D projection) depicting PSD95-immunoreactive clusters (red) on $eGFP^+$ spine-like structures and dendritic shafts in the EPL at 90 dpi in WT and α2-FL mice; co-localization is depicted in yellow (arrowheads). **G-H)** Double immuno-electron microscopy for gephyrin (silver grains, arrowheads) and

eGFP (*) in eGFP$^+$ GCs of α2-FL mice. Each pair of serial sections depicts an asymmetric (excitatory) synapse (arrow) formed by a mitral cell dendritic profile on a eGFP$^+$ GC dendrite profile, which in turn makes a gephyrin-positive (arrowhead) symmetric synapse on the same mitral cell profile. The crossed arrows in H point to an asymmetric synapse onto an eGFP$^-$ spine profile. **I)** Representative traces of spontaneous excitatory currents (sEPSCs) recorded at -70mV at 14 dpi. **J-L)** Histograms of sEPSC frequency (Hz) (J), amplitude (pA) (K), and decay time constant (ms) (L) in GCs from WT and α2-FL mice (mean ± SD). See Tables 4 and 5*B* for statistical analysis; WT and α2-FL groups were compared by one-way ANOVA followed by Bonferroni post tests (* $P < 0.05$).Scale bars: A, C: 5 μm; *F*: 2 μm; G, H: 0.2 μm.

Figure 5: Effects of sensory stimulation and deprivation on spine development in newborn GCs. A) Schematic diagram of the experimental protocol used for olfactory enrichment or deprivation. Adult mice were injected in the SVZ with the eGFP-CRE lentivirus. One week after virus injection, mice were either exposed to enriched olfactory stimuli for 3 weeks or injected with dichlobenil for sensory deprivation. **B)** Representative images of eGFP$^+$ spines on apical dendrites of newborn GCs in enriched (upper panels) and deprived (lower panels) WT and α2-FL mice. **C)** Quantification of spine density (mean ± SEM) in the EPL of deprived and enriched mice. (one-way ANOVA with post-tests; see results section for statistical analysis; *$p < 0.05$). Scale bar: 2 μm.

Figure 6: Effects of early inactivation of *Gabra2* in progenitor cells. A) Schematic diagram of the experimental design: 8-week-old Glast mice were injected with tamoxifen (Tam) or with vehicle (Oil) once a day for five days. At 12 weeks of age, mice were injected with the eGFP-lentivirus in the SVZ; they were then analyzed at 7 or 90 dpi. **B)** Representative images (3-D projections) showing α2-subunit clusters (red) in newborn GCs of Glast mice (Oil and Tam-injected) after 7 dpi, confirmed by colocalization analysis (yellow; arrowheads). Note the loss of α2-subunit clusters in eGFP$^+$ cells of Tam-injected mice. **C)** Quantification of α2-subunit clusters (mean ± SEM) in Tam-injected (green) and Oil mice (grey) at 7 dpi in cell body and in the apical dendrite. **D)** Quantification of α3-subunit and gephyrin clusters (mean ± SEM) in the cell body and apical dendrite of Tam-injected (green) and Oil mice (gray) at 7 dpi, as determined by triple fluorescence staining. There was no significant difference in the density of α3-subunit clusters colocalized with gephyrin (α3/geph) in either compartment. **E)** Representative drawings of eGFP$^+$ cells used for Sholl analysis in Oil (grey) and Tam-injected

Glast mice (green). ***F)*** Histogram of the number of terminal dendritic branches (mean ± SEM) showing a reduction at 7 and 90 dpi in Tam-injected mice. **G)** Sholl analysis comparison between Oil mice (gray line) and Tam-injected mice (green line) at 7 dpi illustrating the reduced dendritic complexity in Tam mice. **H)** Representative images of $eGFP^+$ dendritic spines in the EPL of Oil and Tam-injected mice at 7 and 90 dpi. **I-J)** Histograms of spine density in the EPL (mean ± SEM) at 7 and 90 dpi and PSD95 cluster density on spines and dendritic shaft (clusters/µm dendrite). The decrease of spines correlates with that of PSD95 clusters in Tam-injected mice. Two-tailed Student's t-test; * $p < 0.05$. **K)** Immunofluorescence staining for PSD95 clusters (red) colocalized with $eGFP^+$ spine-like structures and dendritic shafts in the EPL after 7 dpi in Oil control and Tam-injected mice; arrowheads point to sites of colocalization (yellow). Scale bars: B: 10 µm, H: 2 µm; I: 1 µm.

Table 1: List of natural and synthetic odorants used to enrich the olfactory environment

Terragon	Soybean sauce	Juniper berries
Darjeeling tea	(-) Carvon	Cocoa
(–) Limonene	(*) Carvon	Coffee
(+) Limonene	Cinnamon	Vanilla
Rosa	Cumin	Shallot
Chive	Isoamyleacetate	Chocolate
Floreal	Green tea	(+) Limonene
(+) Carvon	Lavender oil	Massale

Table 2: Primary antibodies used in this study

Protein target	Species	Dilution	Source; catalogue Nr	Reference
Doublecortin	Guinea pig	1:2000	Millipore/Chemicon, Temecula, CA; AB2253	(Waclaw et al., 2006)
Gephyrin	Mouse	1:1000	Synaptic Systems, Göttingen, Germany; mAb7a; 147711	(Panzanelli et al., 2009)
GFP	Rabbit Chicken	1:2000 1:5000	Synaptic Systems; 132002 Aves Laboratories, Portland, OR; GFP-1020	(Panzanelli et al., 2009; Duveau et al., 2011)
GAD65	Mouse	1:1000	Developmental Studies Hybridoma Bank, Univ. Iowa; GAD-6	(Chang and Gottlieb, 1988)
$GABA_AR$ α2-subunit	Guinea pig	1:1000	Self-made	(Panzanelli et al., 2011)
PSD95	Mouse	1:1000	UC Davis/NIH NeuroMab; 75-028	(Panzanelli et al., 2009)
TH	Mouse	1:4000	Immunostar, Hudson, WI; 22941	(Holderith et al., 2003)

Table 3: Statistical analysis of synaptic markers in newborn GCs

		Two-way ANOVA	$P_{genotype}$	P_{time}	***Interaction***
α2-subunit	Apical dendrite	$F_{3, 16}$=7.207	0.014	0.170	0.003
	Cell body	$F_{3, 16}$=8.617	<0.0001	0.071	0.001
Gephyrin	Apical dendrite	$F_{3, 16}$=6.703	0.001	0.849	0.004
	Cell body	$F_{3, 16}$=6.622	<0.0001	0.009	0.004
GAD65	Apical dendrite	$F_{3, 16}$=1.561	0.525	<0.0001	0.238
	Cell body	$F_{3, 16}$=0.352	0.292	0.348	0.788

The density of α2-subunit and gephyrin clusters, representing putative postsynaptic sites, as well as $GAD65^+$ puncta, representing presynaptic terminals was analyzed in WT and FL mice. For each genotype, data were further analyzed by one-way ANOVA followed by Dunn's post-test (see main text).

Table 4: Statistical analysis of post-synaptic currents (PSCs)

	Two-way ANOVA	$P_{genotype}$	P_{time}	***Interaction***
eIPSC amplitude	$F_{3,99}$=8.569	<0.0001	<0.0001	0.0001
sIPSC amplitude	$F_{3,75}$=0.876	<0.0001	0.017	0.458
sIPSC frequency	$F_{3,85}$=2.105	0.001	0.014	0.105
sIPSC decay time	$F_{3,63}$=0.243	<0.0001	0.691	0.866
sIPSC rise time	$F_{3,64}$=1.363	0.049	0.011	0.262
sEPSC amplitude	$F_{3,98}$=0.301	0.595	0.348	0.823
sEPSC frequency	$F_{3,95}$=0.981	0.006	0.006	0.405
sEPSC decay time	$F_{3,99}$=1.199	0.772	0.728	0.314
sEPSC rise time	$F_{3,108}$=0.683	0.703	0.04	0.564
Capacitance	$F_{3,126}$=0.815	0.484	0.0011	0.488
Membrane resistance	$F_{3,115}$=1.12	0.052	<0.0001	0.3442
Na^+ current density	$F_{3,122}$=0.579	0.4143	<0.0001	0.630

eIPSCs: evoked inhibitory post synaptic currents; sIPSCs: spontaneous inhibitory post-synaptic currents; sEPSC: spontaneous excitatory post-synaptic currents. Further analysis per genotype and/or time-point is presented in Table 5.

Table 5: Properties of post-synaptic currents

A) Inhibitory post-synaptic currents (IPSCs)

	dpi	WT	α2-FL	*t*-test	MW	Bonferroni
eIPSC amplitude	7	56.86 ± 8.21 n=11	41.15 ± 5.32 n=13	0.113	0.132	ns
(pA)	14	111.80 ± 15.24 n=15	46.60 ± 9.01N=12	0.002**	0.0059**	**
	30	155.70 ± 19.20 n=12	51.04 ± 8.05 n=18	***	***	***
	90	186.01 ± 23.32 n=13	33.78 ± 11.09 n=13	***	***	***
One-way ANOVA		*P=0.0002***	*P=0.1627*			
		7 vs 14 ** ; 7 vs 90***				
sIPSC frequency	7	0.06 ± 0.01 n=9	0.05 ± 0.01 n=12	0.452	0.546	ns
(Hz)	14	0.12 ± 0.03 n=11	0.05 ± 0.01 n=7	0.037*	0.0774	ns
	30	0.10± 0.02 n=15	0.04 ± 0.01 n=17	0.0041**	0.0034**	ns
	90	0.24 ± 0.07 n=15	0.05 ± 0.02 n=7	0.068	0.0048**	**
One-way ANOVA		*P=0.031*	*P=0.1627*			
		*7 vs 90 **				
sIPSC amplitude	7	16.30 ± 2.34 n=9	11.48 ± 0.98 n=8	0.09	0.074	ns
(pA)	14	19.17 ± 1.94 n=12	12.57 ± 0.90 n=9	0.0124*	0.0062**	*
	30	23.46 ± 1.48 n=14	13.93 ± 1.04 n=13	***	***	***
	90	22.90 ± 1.54 n=13	13.81 ± 1.76 n=5	0.0043**	0.0078**	**
One-way ANOVA		*P=0.220*	*P=0.537*			
sIPSC	7	29.29 ± 3.97 n=7	44.27 ± 5.53 n=6	0.0463*	0.0734	ns
decay time constant	14	28.15 ± 2.73 n=12	53.49 ± 12.90 n=7	0.0249*	0.09	*
(ms)	30	33.73 ± 3.30 n=14	54.98 ± 10.33 n=9	0.0305*	0.0298*	*
	90	27.02 ± 3.242 n=13	52.67 ± 5.47 n=3	0.0035**	0.0222*	ns
One-way ANOVA		*P=0.438*	*P=0.889*			
sIPSC	7	0.59 ± 0.05 n=7	0.82 ± 0.06 n=6	0.012*	0.008**	ns
rise time 20-80%	14	0.78 ± 0.07 n=12	0.95 ± 0.08 n=7	0.119	0.139	ns
(ms)	30	0.68 ± 0.07 n=14	0.70 ± 0.04 n=9	0.815	0.378	ns
	90	0.64 ± 0.04 n=13	0.62 ± 0.15 n=4	0.841	0.533	ns
One-way ANOVA		*P=0.28*	*P=0.0263**			

B) Excitatory post-synaptic currents (EPSCs)

	dpi	WT	α2-FL	*t*-test	MW	Bonferroni
sEPSC frequency	7	11.48 ± 0.74 n=11	1.12 ± 0.27 n=11	0.653	0.5546	ns
(Hz)	14	4.43 ± 0.82 n=12	1.78 ± 0.58 n=11	0.0175*	0.0151*	*
	30	5.42 ± 0.94 n=12	3.13 ± 0.52 n=19	0.028*	0.0744*	*
	90	3.87 ± 0.68 n=11	2.21 ± 0.67 n=16	0.1051	0.0543	ns
One-way ANOVA		*0.021***	*0.126*			
		*7 vs 14 *; 7 vs 30***				
sEPSC amplitude	7	8.88 ± 0.91 n=11	8.35 ± 1.10 n=11	0.7147	0.4307	ns
(pA)	14	9.31 ± 1.36 n=12	9.37 ± 0.62 n=13	0.968	0.849	ns
	30	8.64 ± 0.84 n=14	9.38 ± 0.88 n=19	0.5561	0.392	ns
	90	7.26 ± 0.37 n=12	8.33 ± 0.65 n=14	0.1819	0.2077	ns
One-way ANOVA		*0.583*	*0.251*			
sEPSC	7	7.58 ± 1.57 n=11	9.57 ± 1.31 n=10	0.3471	0.1698	ns
decay time constant	14	9.61 ± 1.76 n=13	8.69 ± 1.63 n=13	0.7036	0.7976	ns
(ms)	30	9.46 ± 1.37 n=14	10.79 ± 1.65 n=19	0.5586	0.8698	ns
	90	12.16 ± 2.41 n=11	8.36 ± 1.25 n=16	0.1414	0.1671	ns
One-way ANOVA		*0.2673*	*0.718*			
sEPSC	7	1.03 ± 0.05 n=11	0.98 ± 0.06 n=15	0.5043	0.6037	ns
rise time 20-80%	14	0.90 ± 0.05 n=13	0.82 ± 0.042 n=16	0.2173	0.3131	ns
(ms)	30	0.83 ± 0.06 n=14	0.78 ± 0.06 n=19	0.5617	0.6229	ns
	90	0.87 ± 0.04 n=12	0.98 ± 0.13 n=16	0.506	0.9815	ns
One-way ANOVA		*0.0775*	*0.1314*			

eIPSCs: Evoked inhibitory post synaptic currents. sIPSCs: Spontaneous inhibitory post-synaptic currents. sEPSC: Spontaneous excitatory post-synaptic currents. Values are mean ± SEM. General statistics are presented in Table 4. Each genotype was analyzed by one-way ANOVA followed by Dunns post-test (ns $P>0.05$; * $P<0.05$; ** $P<0.01$). WT and FL groups were compared two-by-two by Student's *t*-test and Mann Whitney test (MW).

Table 6: Intrinsic membrane properties of newborn GCs

	dpi	WT	α2-FL	*t*-test	MW	Bonferroni
Cm (pF)	7	12.09 ± 1.42 n=13	11.40 ± 0.89 n=16	0.6727	0.8608	ns
	14	13.70 ± 0.86 n=17	12.49 ± 0.80 n=16	0.3148	0.3219	ns
	30	10.70 ± 0.74 n=17	11.86 ± 0.85 n=19	0.3188	0.2347	ns
	90	10.07 ± 0.91 n=15	9.07 ± 0.61 n=21	0.3487	0.4703	ns
One way ANOVA		*P=0.06*	*P=0.0099***			
			*14 vs 90**			
Rm (Gohm)	7	1.37 ± 0.14 n=13	1.80 ± 0.28 n=14	0.1992	0.6979	ns
	14	0.79 ± 0.09 n=16	0.76 ± 0.071 n=16	0.8536	0.8358	ns
	30	0.73 ± 0.10 n=16	0.80 ± 0.12 n=17	0.6823	0.8712	ns
	90	0.67 ± 0.08 n=14	0.90 ± 0.10 n=16	0.0775	0.0504	ns
One way ANOVA		*P=0.006***	*P=0.0026***			
		*7 vs 14 *; 7 vs 30**; 7 vs 90***	*7 vs 14 **; 7 vs 30***			
iNa^+ (pA/pF)	7	87.08 ± 18.49 n=12	93.68 ± 13.96 n=16	0.7734	0.6260	ns
	14	141.0 ± 14.32 n=17	146.1 ± 12.47 n=16	0.7893	0.6787	ns
	30	179.2 ± 15.36 n=17	168.4 ± 18.59 n=19	0.6610	0.4661	ns
	90	174.6 ± 21.65 n=11	158.5 ± 22.92 n=17	0.6338	0.5409	ns
One way ANOVA		*0.0036***	*0.0192**			
		*7 vs 30**; 7 vs 90**	*7 vs 30**			

Cm: membrane capacitance; Rm; membrane resistance; iNa^+: density of voltage-dependant Na^+ channels-mediated currents (normalized to Cm). Values are mean ± SEM. General statistics are presented in Table 4. Each genotype was analyzed by one-way ANOVA followed by Dunn's post-test (ns, P>0.05; * P<0.05; **P<0.01). For a given time-point WT and FL groups were compared two-by-two by Student's *t*-test and Mann Whitney test (MW).

Table 7: Statistical analysis of dendrite morphology

A) Sholl analysis

DPI	**Genotype**	***n***	**Area under the curve**		
			mean±SD	*t*	*P*
7	WT	3	233±16	t_4= 0.412	ns
	FL	3	224±12		
14	WT	3	237±19	t_4= 0.172	ns
	FL	3	240±7		
30	WT	3	410±22	t_4= 3.748	0.02
	FL	3	262±32		
90	WT	3	385±7	t_4= 6.954	0.002
	FL	3	289±12		

B) Dendrite topology and spine density

	Two-way ANOVA	$P_{genotype}$	P_{time}	***Interaction***
GCL spine density	$F_{4, 20}$=9.164	0.000	<0.0001	0.000
EPL spine density	$F_{3, 16}$=5.542	<0.0001	<0.0001	0.01
Number of terminal branches	$F_{3, 16}$=5.887	0.0001	0.0009	0.007
Total dendritic tree length	$F_{3, 16}$=1.506	0.003	<0.0001	0.251

For the Sholl analysis, pair-wise comparison was performed by unpaired Student's t-test. Differences in dendrite topology and spine densities were analyzed further by one-way ANOVA followed by Dunn's post-test for each genotype (see main text).

Fig. 1

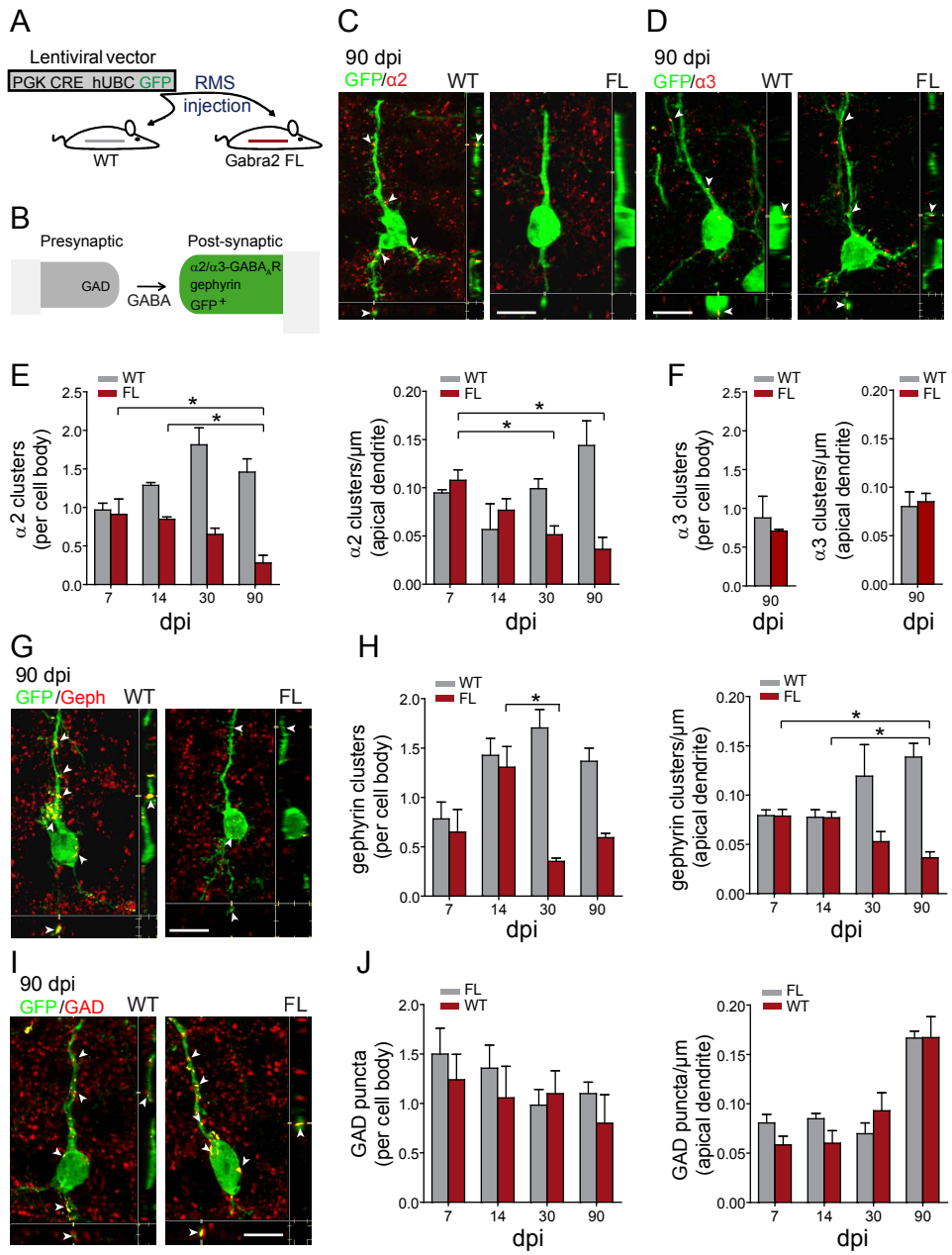
A
Lentiviral vector
PGK CRE hUBC GFP
RMS
injection
WT
Gabra2 FL
B
Presynaptic
Post-synaptic
GAD
GABA
α2/α3-GABA$_A$R
gephyrin
GFP+
C
90 dpi
GFP/α2
WT
FL
D
90 dpi
GFP/α3
WT
FL
E
WT
FL
α2 clusters (per cell body)
α2 clusters/µm (apical dendrite)
dpi
F
α3 clusters (per cell body)
α3 clusters/µm (apical dendrite)
dpi
G
90 dpi
GFP/Geph
WT
FL
H
gephyrin clusters (per cell body)
gephyrin clusters/µm (apical dendrite)
dpi
I
90 dpi
GFP/GAD
WT
FL
J
FL
WT
GAD puncta (per cell body)
GAD puncta/µm (apical dendrite)
dpi

Fig 2

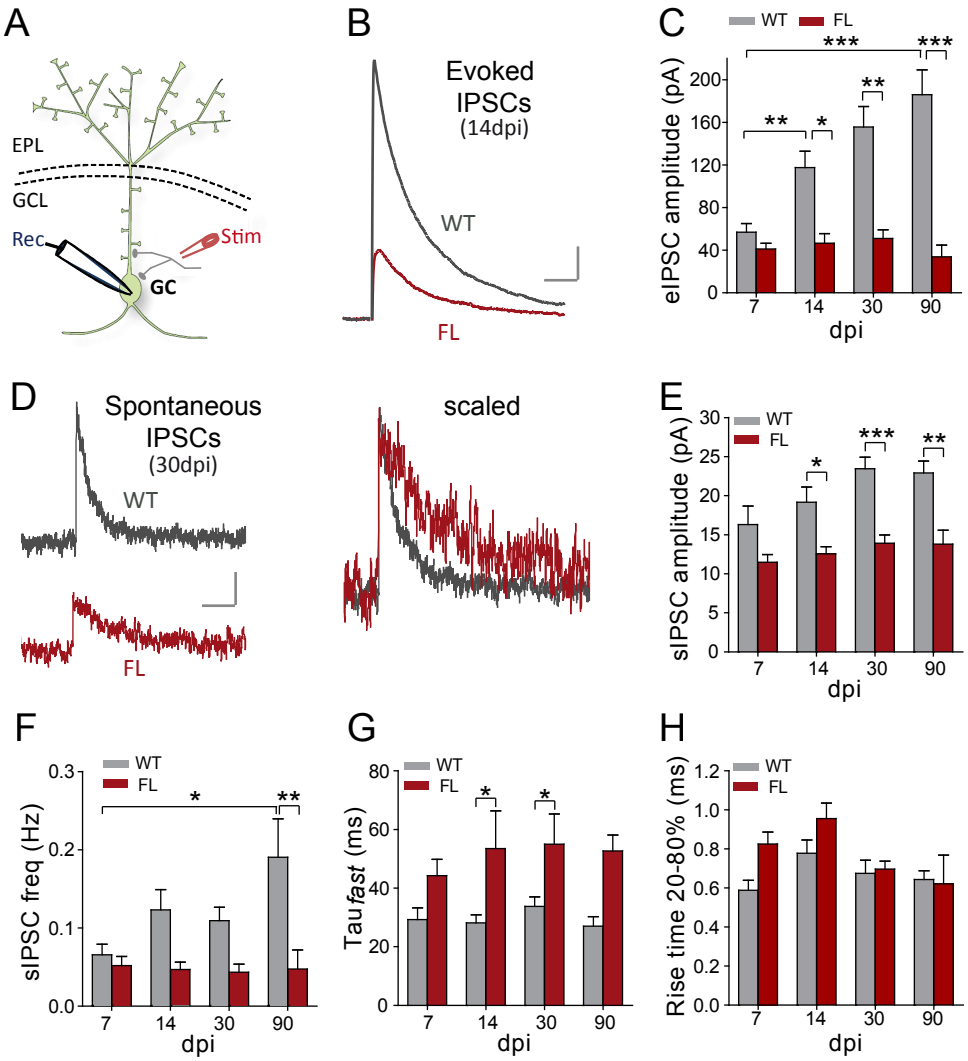
A
EPL
GCL
Rec
Stim
GC
B
Evoked
IPSCs
(14dpi)
WT
FL
C
WT
FL
eIPSC amplitude (pA)
dpi
D
Spontaneous
IPSCs
(30dpi)
WT
FL
scaled
E
sIPSC amplitude (pA)
dpi
F
sIPSC freq (Hz)
dpi
G
Tau fast (ms)
dpi
H
Rise time 20-80% (ms)
dpi

Fig. 3

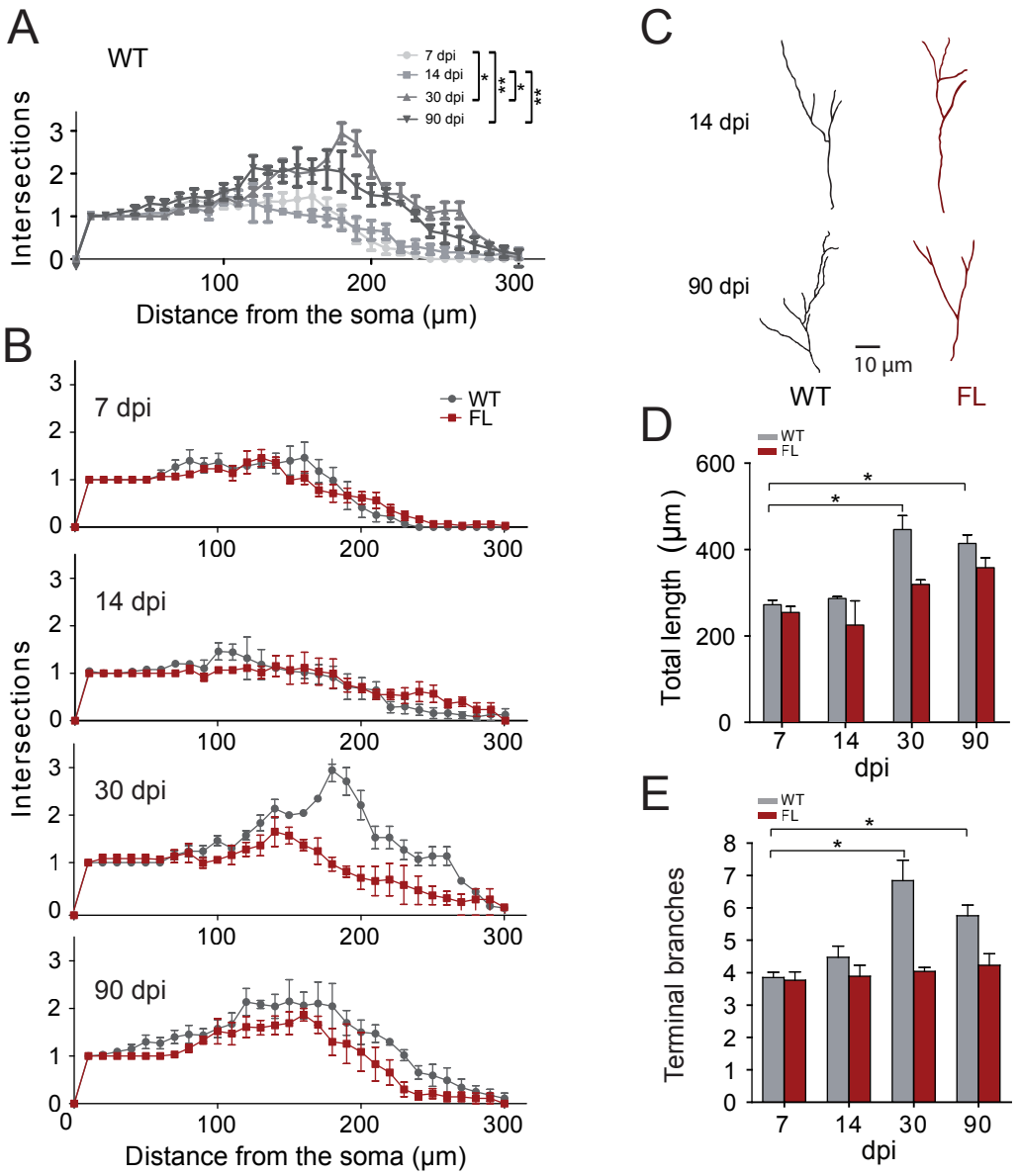
A
WT
7 dpi
14 dpi
30 dpi
90 dpi
Intersections
Distance from the soma (μm)
B
7 dpi
14 dpi
30 dpi
90 dpi
WT
FL
Intersections
Distance from the soma (μm)
C
14 dpi
90 dpi
10 μm
WT
FL
D
Total length (μm)
dpi
E
Terminal branches
dpi

Fig. 4

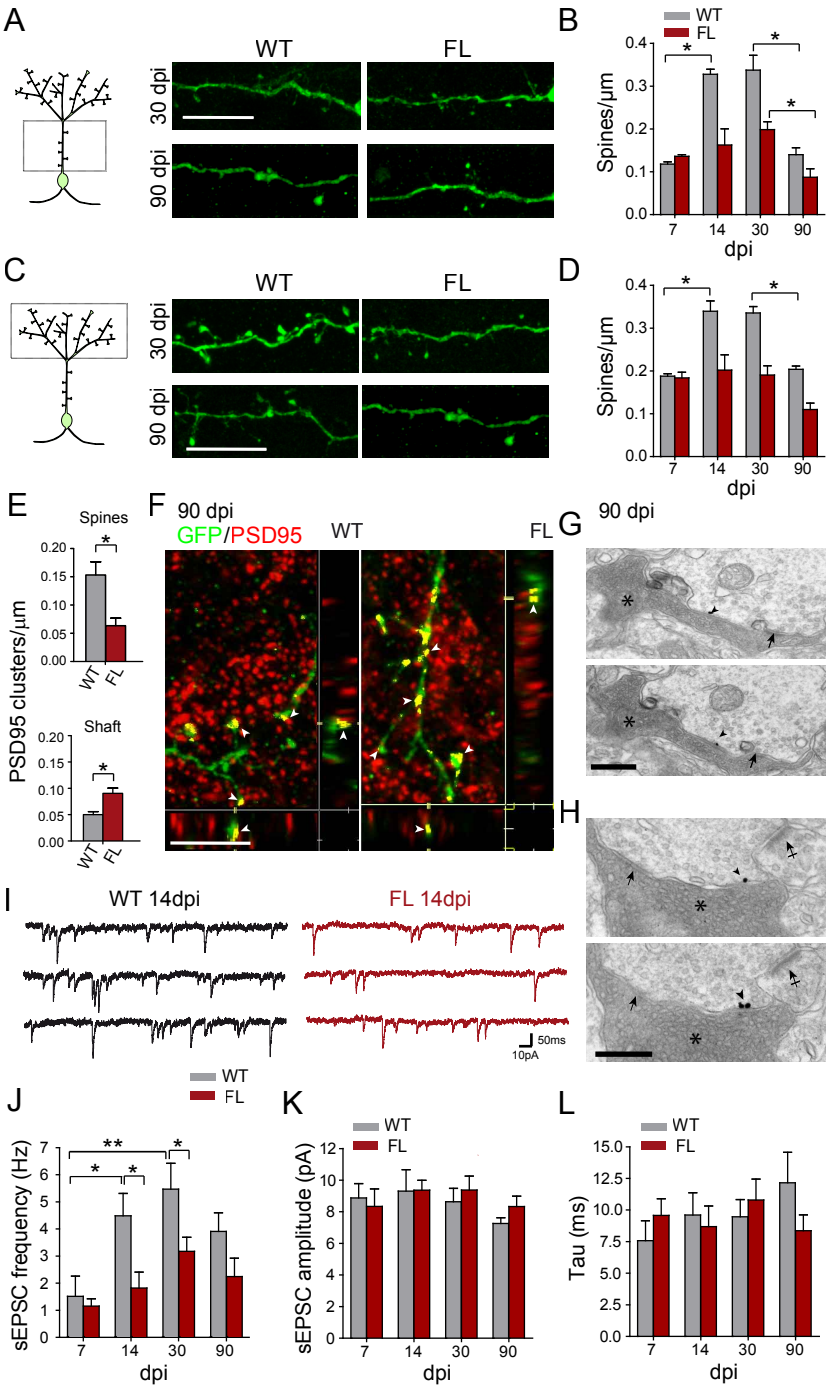
A
WT
FL
30 dpi
90 dpi
B
WT
FL
Spines/µm
dpi
C
D
E
Spines
Shaft
PSD95 clusters/µm
F
90 dpi
GFP/PSD95
G
90 dpi
H
I
WT 14dpi
FL 14dpi
50ms
10pA
J
sEPSC frequency (Hz)
K
sEPSC amplitude (pA)
L
Tau (ms)

Fig 5

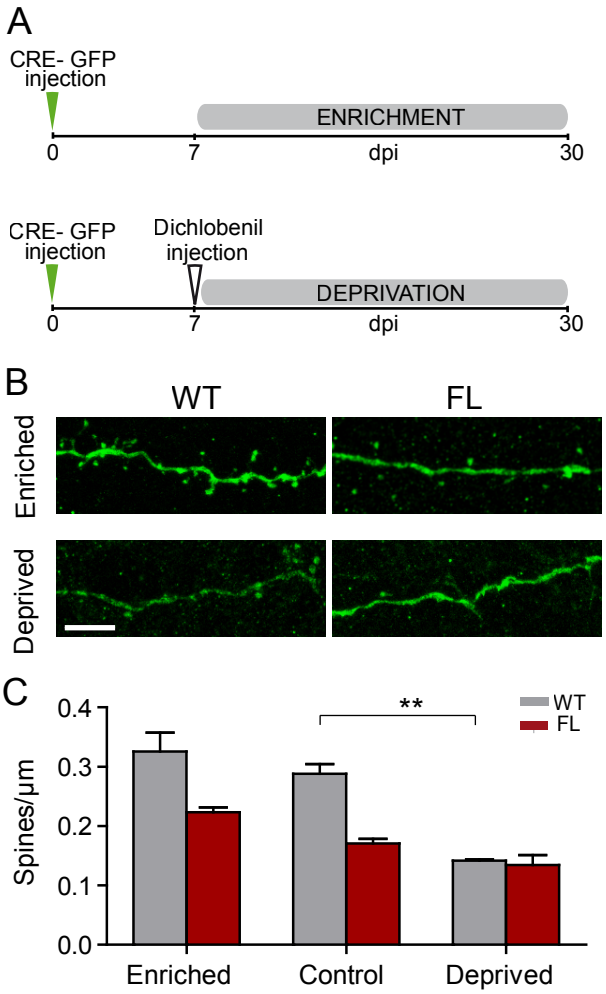
A
CRE- GFP injection
ENRICHMENT
0
7
dpi
30
CRE- GFP injection
Dichlobenil injection
DEPRIVATION
0
7
dpi
30
B
WT
FL
Enriched
Deprived
C
Spines/µm
0.4
0.3
0.2
0.1
0.0
**
WT
FL
Enriched
Control
Deprived

Fig 6

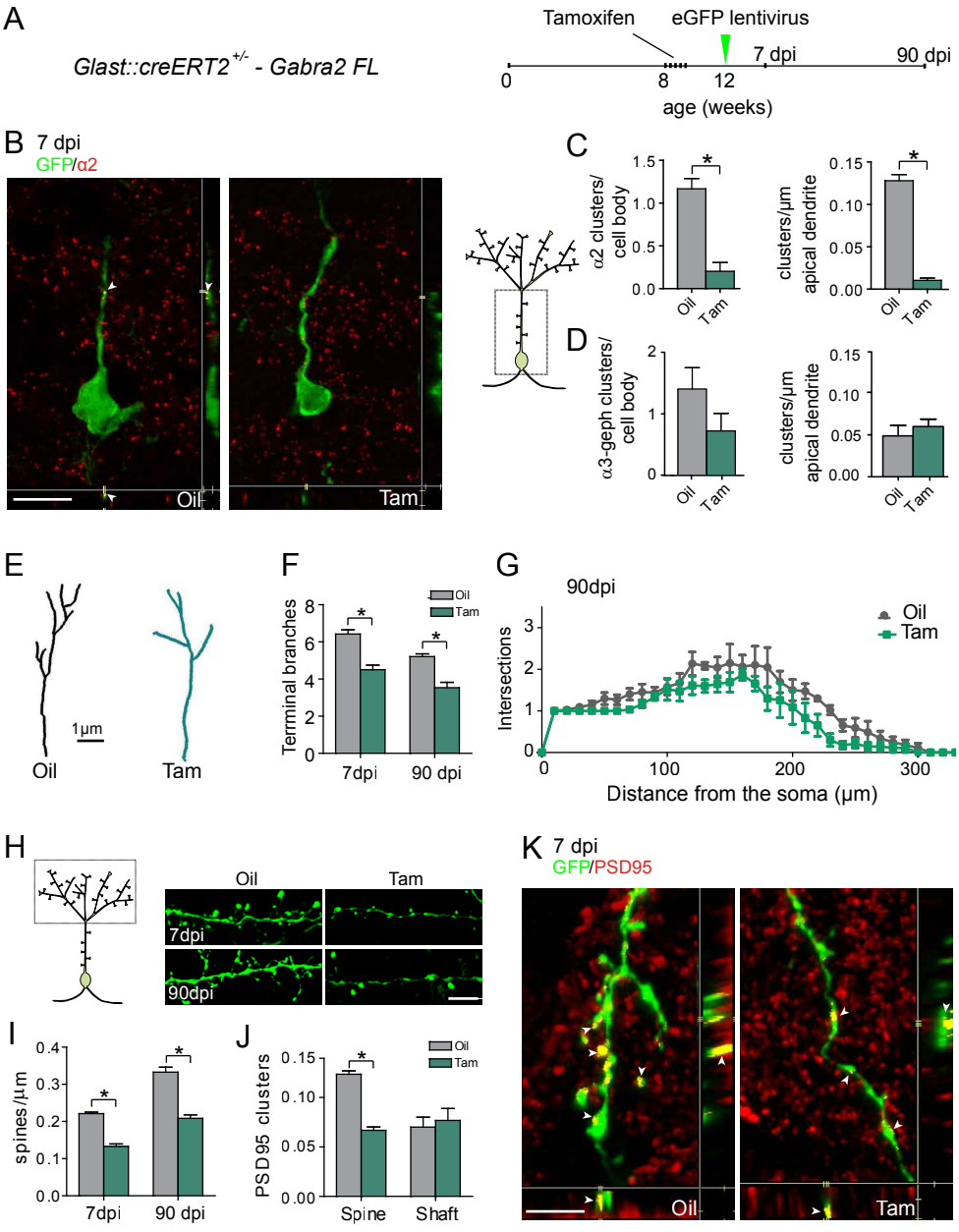
A
Glast::creERT2 +/- - Gabra2 FL
Tamoxifen
eGFP lentivirus
7 dpi
90 dpi
0
8
12
age (weeks)
B 7 dpi
GFP/α2
Oil
Tam
C
α2 clusters/ cell body
clusters/µm apical dendrite
D
α3-geph clusters/ cell body
clusters/µm apical dendrite
E
1µm
Oil
Tam
F
Terminal branches
7dpi
90 dpi
G
90dpi
Intersections
Distance from the soma (µm)
H
7dpi
90dpi
I
spines/µm
J
PSD95 clusters
Spine
Shaft
K 7 dpi
GFP/PSD95